

Atmospheric Measurement Techniques Discussions is the access reviewed discussion forum of *Atmospheric Measurement Techniques*

**Laboratory-
generated primary
marine aerosol**

E. Fuentes et al.

Laboratory-generated primary marine aerosol via bubble-bursting and atomization

E. Fuentes¹, H. Coe¹, D. Green², and G. McFiggans¹

¹Centre for Atmospheric Sciences, School of Earth, Atmospheric and Environmental Sciences, Manchester M13 9PL, UK

²Scottish Association for Marine Science, Oban, UK

Received: 7 September 2009 – Accepted: 15 September 2009

– Published: 29 September 2009

Correspondence to: G. McFiggans (g.mcfiggans@manchester.ac.uk)

Published by Copernicus Publications on behalf of the European Geosciences Union.

Title Page

Abstract

Introduction

Conclusions

References

Tables

Figures

◀

▶

◀

▶

Back

Close

Full Screen / Esc

Printer-friendly Version

Interactive Discussion

Abstract

A range of bubble and sea spray aerosol generators has been tested in the laboratory and compared with ocean measurements. We have shown that the method of generation has a significant influence on the properties of the aerosol particles produced.

Hence, the validity of a generation system to mimic atmospheric aerosol is dependent on its capacity of generating bubbles and particulate in a realistic manner. A bubble-bursting aerosol generator consisting in the production of bubbles by the impingement of water jets on seawater was shown to best reproduce the real oceanic bubble and aerosol distributions signatures.

Two aeration methods and a plunging-water jet system were tested as bubble-bursting aerosol generators for comparison with a standard nebulizer. The methods for aerosol production were evaluated by analysing the bubble spectrum generated by the bubble-bursting systems and the submicron size distribution, hygroscopicity and cloud condensation nucleus activity of the aerosols generated by the different techniques. Significant differences in the bubble spectrum and aerosol properties were observed when using different aerosol generators.

The hygroscopicity and cloud condensation nucleus activity of aerosols generated by the different methods were similar when a sample of purely inorganic salts was used as a parent seawater solution; however, significant differences in the aerosol properties were found when biogenic organics were incorporated in the seawater samples. The presence of organics in the aerosol caused suppression of the growth factor at humidities above 75% RH and an increase in the critical supersaturation when compared with the case without organics. Unequal extent of these effects was observed for aerosols generated by the different methods of particle production. While the highest reductions of the growth factor were observed for the plunging-water jet aerosol, the largest effect on the critical supersaturation was obtained for the atomization-generated particles. The results of this work show that the aerosol generation mechanism affects the particles organic enrichment, thus the behaviour of the produced aerosols strongly

AMTD

2, 2281–2320, 2009

Laboratory-generated primary marine aerosol

E. Fuentes et al.

Title Page

Abstract

Introduction

Conclusions

References

Tables

Figures

◀

▶

◀

▶

Back

Close

Full Screen / Esc

Printer-friendly Version

Interactive Discussion



depends on the laboratory aerosol generator employed.

1 Introduction

Marine aerosol accounts for the majority of the global natural aerosol loading and consequently, has an important impact on the Earth's radiative budget and biogeochemical cycling (O'Dowd et al., 2004, 2007). Aerosol particles affect the radiative balance of the atmosphere by absorbing and scattering in-coming solar radiation (direct effect) and by affecting the microphysical properties of clouds (indirect effect). The indirect effect is a significant source of uncertainty due to the complexity of the atmospheric interactions involved, as well as the wide range of scales in which these interactions occur (Ramaswamy et al., 2001).

Sea-salt primary aerosols are produced as a result of breaking wave processes occurring on oceans surfaces. For wind speeds higher than 4 m s^{-1} waves generated as a result of wind stress break and sea-salt droplets with diameters up to $10 \mu\text{m}$ are formed (O'Dowd et al., 1997). Breaking waves dissipate up to 40% of their energy and up to 50% of the energy loss is expended in entraining air in the water bulk and creating a dense plume of bubbles (Rapp and Melville, 1990). The formed bubbles rise and burst upon reaching the surface, thereby producing the so-called film and jet drops. Depending on its size, a bubble can produce about ten jet drops with an average diameter of $1\text{--}2 \mu\text{m}$ and several hundred of film drops with a diameter smaller than $1 \mu\text{m}$ as a result of bubble bursting (O'Dowd et al., 1997). The sea salt aerosol total number concentration is normally dominated by particles in the submicron size range from 5 to 300 nm, with a decline in the particle number with increasing size (Fitzgerald, 1991).

The primary marine aerosol is composed of seawater enriched with inorganic and organic chemical compounds as well as with bacteria and viruses (Boehme et al., 1993). Both natural (biogenic) and anthropogenic compounds, dissolved in the near-surface layer of the ocean or as a thin film on the ocean surface, may contribute to the content of marine aerosols. Under breaking wave conditions, the primary mechanism of

Laboratory-generated primary marine aerosol

E. Fuentes et al.

Title Page

Abstract

Introduction

Conclusions

References

Tables

Figures

◀

▶

◀

▶

Back

Close

Full Screen / Esc

Printer-friendly Version

Interactive Discussion



Laboratory-generated primary marine aerosol

E. Fuentes et al.

Title Page

Abstract

Introduction

Conclusions

References

Tables

Figures

◀

▶

◀

▶

Back

Close

Full Screen / Esc

Printer-friendly Version

Interactive Discussion

transport of biogenic surfactants to the ocean surface is by bubble scavenging. When the bubbles reach the water surface, the organics concentrated on their surface are ejected into the atmosphere along with dissolved inorganic constituents of seawater. Thereby, the seawater composition, bubble spectrum, bubble hydrodynamics and the formation and chemical composition of the aerosol are closely interrelated and interdependent (Duce and Hoffman, 1976; Keene et al., 2007; Tseng et al., 1992). Chemical analysis of sea salt particles collected in field experiments has provided evidence for the presence of significant concentrations of biogenic organic matter in areas with high biological activity. This organic matter originates from the metabolic activity of oceanic phytoplankton and consists of a complex mixture of dissolved and particulate species, including a variety of organic compounds such as carboxylic acids, lipids, amino acids and carbohydrates (Aluwihare and Repeta, 1999). The presence of this organic material in seawater might influence the aerosol production mechanism, by affecting the bubble hydrodynamics, and also the behaviour of the aerosol generated, since this organic matter is likely to have an effect on the hygroscopic growth and the cloud condensation activity of the particles (McFiggans et al., 2006).

A number of laboratory investigations have been conducted in order to study a range of physical and chemical characteristics of marine aerosols, such as size distribution, reactivity, hygroscopicity and cloud activation properties (Braban et al., 2007; Mårtensson et al., 2003; Niedermeier et al., 2007; Saul et al., 2006; Stewart and Cox, 2004; Svenningsson et al., 2005). It is a common practice to use atomizers for the generation of laboratory marine aerosol proxies from seawater samples (Braban et al., 2007; McNeill et al., 2006; Niedermeier et al., 2007; Riziq et al., 2006; Saul et al., 2006; Svenningsson et al., 2005; Taketani et al., 2009), while only in a few works the aerosol has been produced by bubble-bursting via aeration through glass frits or diffusers (Cloke et al., 1991; Keene et al., 2007; Mårtensson et al., 2003; Tyree et al., 2007; Wise et al., 2009) or using water jets (Cipriano and Blanchard, 1981; Facchini et al., 2008; Sellegri et al., 2006).

The production of sea salt particles by bubble bursting has been simulated in labo-



ratory works to study the marine aerosol size distribution properties. Mårtensson et al. (2003) and Tyree et al. (2007) reproduced the typical marine aerosol size distribution signature by bubbling artificial seawater through different porous media; however, the shape of the bubble spectrum obtained in these works did not completely resemble the oceanic bubble spectrum shape. Sellegri et al. (2006) compared the bubble spectrum and the submicron aerosol size distributions generated by bubble bursting using a water recirculation system and aeration through glass frits of different porosity. Whereas only the bubble spectrum produced by the recirculation system matched the oceanic bubble spectrum size range, the particle size distributions obtained using the different bubbling systems showed a dominant peak around 100 nm diameter and a second mode at 300–400 nm, most evident in the waterfall system. Some of these investigations on sea salt size distributions also studied the effect of salinity, water temperature (Mårtensson et al., 2003; Tyree et al., 2007; Sellegri et al., 2006) and organic matter by using organic proxies, such as oleic acid (Tyree et al., 2007) and sodium dodecyl sulphate (SDS) (Sellegri et al., 2006).

Although most marine aerosol size distribution studies have given emphasis to the reproduction of particle formation via bubble bursting, the majority of investigations on the aerosol behaviour, such as halogens reactivity (Braban et al., 2007), N_2O_5 uptake (McNeill et al., 2006; Stewart and Cox, 2004; Saul et al., 2006), hygroscopic growth (Niedermeier et al., 2007; Svenningsson et al., 2005) and cloud condensation nucleus activity (Svenningsson et al., 2005) use atomizers as aerosol generators. The real process for marine aerosol formation greatly differs from the aerosol generation induced by the atomization mechanism; however, the extent to which the discrepancy between this technique and the real production processes can affect the aerosol behaviour has not been analysed. The reliability of laboratory aerosol studies depends on the degree to which the aerosol laboratory proxies are able to mimic the behaviour of real aerosols. The properties of such aerosol proxies might be dependent on the generation mechanisms used in the laboratory; however, none of the previously conducted investigations specifically addresses the performance of different laboratory methods as generators

Laboratory-generated primary marine aerosol

E. Fuentes et al.

Title Page

Abstract

Introduction

Conclusions

References

Tables

Figures

◀

▶

◀

▶

Back

Close

Full Screen / Esc

Printer-friendly Version

Interactive Discussion



of marine aerosol.

Although the dominant mass fraction of sea spray aerosol is inorganic sea salt, organic matter can also contribute to the overall mass (O'Dowd et al., 2007). During high biological activity periods organic matter has been shown to be the dominant component of the submicron marine aerosol, comprising approximately 63% of the total aerosol mass in the submicron size range (O'Dowd et al., 2004). The role of such organic matter on the behaviour of the marine aerosols remains largely uncertain; hence further laboratory investigations on sea spray aerosol containing biogenically derived organic matter are needed to clarify the effect of this material on the aerosol properties. It is likely that both the amount and size fractionation of the organic matter incorporated into the marine aerosol are affected by the mechanism employed for aerosol generation. The use of different aerosol generators may lead to the production of aerosols with varying chemical composition and thus, to a diverging interpretation of the experimental results. Therefore, it is important to determine the impact of the generation techniques on the laboratory synthesized aerosols.

This work presents an experimental study based on the characterization of sea salt aerosol particles generated from artificial and natural seawater by using different laboratory techniques. The aim of this investigation is to assess the sensitivity of the aerosol properties to the generation methods applied and the ability of the employed techniques for producing representative marine aerosol particles. Two aeration methods and a plunging-water jet system were tested as bubble-bursting aerosol generators and compared with a standard nebulizer. The ability of the bubble-bursting techniques to reproduce the real oceanic bubble spectrum signature was analysed by means of a series of optical bubble spectrum measurements. Additionally, the size distribution of the aerosols created by bubble bursting and atomization were compared with existing real particle size distributions. Measurements of water uptake and cloud condensation nucleus activity (CCN) of the aerosol produced from artificial and natural seawater containing biogenic organics were conducted in order to elucidate the extent to which the different techniques employed for aerosol production influence the behaviour of the

Laboratory-generated primary marine aerosol

E. Fuentes et al.

Title Page

Abstract

Introduction

Conclusions

References

Tables

Figures

◀

▶

◀

▶

Back

Close

Full Screen / Esc

Printer-friendly Version

Interactive Discussion



generated aerosols.

2 Experimental

2.1 Aerosol generation

Bubble-bursting experiments were performed using a PTFE tank (30.5×20.3×21.4 cm) of 10 l capacity. The tank was filled with 6 l of seawater proxy, which corresponds to a height of 13 cm. Bubble-bursting aerosol formation was simulated by generating bubbles in the bulk of seawater samples using different techniques (Fig. 1). Two systems were employed for the production of bubbles in the tank via aeration: a sintered glass filter (Fisher Sci., 20 μm mean pore size) and an aquarium diffuser (Elite Aquarium air stone, unknown pore size) through which zero air was forced for bubble generation in the water bulk. The glass sintered filter and the aquarium diffuser were placed at 5 and 13 cm below the water surface, respectively.

A method consisting of the recirculation of water by means of a peristaltic pump was additionally used as bubble-bursting aerosol generator. By using this technique, a plunging water jet was continuously created in the center of the tank, thereby causing the air entrained in the water bulk to disperse in a plume of bubbles that burst upon reaching the water surface. A single water jet was created for the bubble spectrum measurements. In order to generate a statistically significant number of particles for the aerosol experiments, the water flow was divided in eight water jets by using a flow distributor. A chemically resistant Teflon composite tube (Masterflex I/P 70) was employed for water recirculation in order to avoid contamination of the water samples and adhesion of surfactants on the tubing wall. The water flow was controlled by setting the peristaltic pump rotating speed in a range of 20–40 rpm and monitored using a rotameter. The bubble plume penetration distance was from 7 to 10 cm, depending on the water recirculation flow selected.

For the aerosol experiments the PTFE tank was sealed and vented with a continu-

Laboratory-generated primary marine aerosol

E. Fuentes et al.

Title Page

Abstract

Introduction

Conclusions

References

Tables

Figures

⏪

⏩

◀

▶

Back

Close

Full Screen / Esc

Printer-friendly Version

Interactive Discussion



ous air flow of 3 lpm. The humidity of the flow directed from the tank to the aerosol characterization instruments was reduced down to 32–42% RH by mixing the sample with a 5% volumetric dry air flow, monitored by a mass flow controller, and by using a Nafion gas dryer.

5 Thorough cleaning procedures were applied in order to minimize the presence of contaminants in the system. An isopropanol and deionised water solution was first recirculated in the PTFE tank and air forced through the porous units for an hour, followed by two sequential tank washes with 5 l of deionised water. Next the tank walls and bubbling apparatus were rubbed with chloroform, rinsed and washed with
10 deionised water. In order to rinse the pump tubing and the aeration units, deionised water was recirculated through the tank tubing and air was forced through the aeration stones immersed in water. Finally, the tank was washed twice with 5 l of deionised water.

For the nebulisation experiments a TOPAS atomizer aerosol generator (ATM 226)
15 was used. In the atomization method a flow of compressed air is introduced in the liquid vessel through the atomizer nozzle, producing a high velocity jet at expansion. As a result of the Bernoulli effect, the aqueous solution is drawn from the atomizer vessel and subsequently, a high-velocity air flow breaks up the solution into droplets and suspends the droplets in the flow, forming the aerosol. Atomization of deionised water
20 and rinsing with isopropanol, chloroform and deionised water were applied for cleaning and washing the atomizer vessel and tubing prior the nebulisation experiments.

2.2 Materials and methods

Artificial seawater was prepared from analytical grade salts and deionised water following the method described by Kester et al. (1967) so that the ionic mass ratios of Na^+ , Cl^- , Mg^{2+} , HCO_3^- and SO_4^{2-} were comparable to those in seawater. The salt mixture
25 contained, by mass, 73.6% NaCl, 14.5% MgCl_2 , 11.5% Na_2SO_4 and 0.004% NaHCO_3 . Seawater samples of 35‰ salinity were prepared by adjusting the solution density to 1025 kg m^{-3} at 20°C using a hydrometer.

Laboratory-generated primary marine aerosol

E. Fuentes et al.

Title Page

Abstract

Introduction

Conclusions

References

Tables

Figures

◀

▶

◀

▶

Back

Close

Full Screen / Esc

Printer-friendly Version

Interactive Discussion



Laboratory-generated primary marine aerosol

E. Fuentes et al.

Natural seawater solutions containing phytoplankton-released organics were prepared for the hygroscopicity and CCN activity experiments. The organic material was biogenically-synthesized by culturing *Thalassiosira Rotula* diatom cells in the laboratory. Algal growth media was prepared with GF/C (Whatman) filtered aged natural seawater collected from the Tiree passage (Scotland, UK), amended with F/2 nutrients and either selenite or silicate (Guillard, 1975), and sterilised by autoclaving (121°C for 15 min). The algal cultures were grown in glass Erlenmeyer flasks fitted with gas permeable stoppers or 20 l polycarbonate carboys (Nalgene) at 15°C with a photon flux density of ca. 70 $\mu\text{mol PAR m}^{-2} \text{s}^{-1}$ supplied by cool-white fluorescent lighting (Phillips, Netherlands) with a photoperiod of 12:12 h (light:dark). Following algal growth in Erlenmeyer flasks, the cell biomass was removed by filtration through pre-combusted (450°C for 8 h) glass fiber filters (GF/F; Whatman) and subsequently through dionised-water rinsed and sterile polycarbonate filters (0.2 μm ; Millipore). Large volume algal cultures (10–20 l) were subjected to cross-flow filtration (0.2 μm ; Schleicher and Schuell) to remove algal and bacterial biomass. The algal organic material was then stored at –20°C and kept frozen until use.

For analysis of the organic content (DOC) the seawater samples were aspirated from the filtrate using acid-washed glass pipettes to pre-combusted glass ampules or autosampler bottles and acidified with orthophosphoric acid and stored in the dark at 4°C until analysis. DOC and total nitrogen (TN) analyses were conducted as per standard procedures on a Shimadzu TOC-V CPH/CPN fitted with a TNM-1 module for simultaneous nitrogen measurement.

2.3 Bubble spectrum measurements

The size distribution of bubbles generated in the tank was measured with an optical bubble spectrometer (TNO-miniBMS) in the diameter size range from 30 to 1140 μm . The system consists of a CCD camera which records images of the bubbles generated in the water bulk in a sample volume of 110 mm^3 illuminated by a light source. The CCD camera was equipped with a daylight blocking filter and a telescope consisting of

[Title Page](#)[Abstract](#)[Introduction](#)[Conclusions](#)[References](#)[Tables](#)[Figures](#)[⏪](#)[⏩](#)[◀](#)[▶](#)[Back](#)[Close](#)[Full Screen / Esc](#)[Printer-friendly Version](#)[Interactive Discussion](#)

two lenses, with focal lengths 40 and 80 mm (Leifer et al., 2003).

Images acquired by the CCD camera were analysed by image processing software to obtain the bubble size histograms. Bubble size was determined by discriminating the bubble image from the background by image thresholding assuming a spherical bubble shape, while the sample volume and bubble size calibration allowed the calculation of the bubble size distribution.

The measurements were made on the rising column of bubbles at circa 3–8.5 cm below the water surface and each bubble spectrum was averaged on the images recorded over 2 min. Artificial seawater solutions were used to perform these experiments with the different bubbling systems. The experimental set-up for the bubble spectrum measurements is illustrated in Fig. 1a and b for the plunging-water jet and the aeration systems, respectively. All experiments were carried out at room temperature in the range 15–20°C.

2.4 Aerosol characterization

The size distribution of the generated aerosols was measured using a Differential Mobility Particle Sizer (DMPS). The DMPS consists of two Vienna design Differential Mobility Analysers (DMAs) (Williams, 1999; Williams et al., 2007): an ultrafine DMA for particles in the size range 3.4–34 nm and a standard DMA for particle sizes from 30–830 nm. After transmission through the DMAs, particles are counted using condensation particle counters (CPC). The ultrafine DMA was attached to a TSI 3025A CPC counter and the standard DMA to a TSI 3010 CPC particle counter. The DMAs were operated in parallel and utilised a custom built sealed, recirculating sheath air system, which was humidity controlled and filtered. Particle size distributions in the diameter size range from 3 to 450 nm were obtained as the average of 6 scans during a 60 min measurement period.

A dual-column continuous flow CCN counter (Droplet Measurement Technologies) combined with a Vienna designed DMA and a particle counter TSI 3010 CPC were employed to characterize the aerosol cloud condensation activity. The DMA was used

Title Page

Abstract

Introduction

Conclusions

References

Tables

Figures



Back

Close

Full Screen / Esc

Printer-friendly Version

Interactive Discussion



Laboratory-generated primary marine aerosol

E. Fuentes et al.

Title Page

Abstract

Introduction

Conclusions

References

Tables

Figures

◀

▶

◀

▶

Back

Close

Full Screen / Esc

Printer-friendly Version

Interactive Discussion



to generate monodisperse aerosol in the size range between 40 and 100 nm dry diameter. These particles were directed in parallel to the CPC and CCN counters. The CCN counter sample flow was 0.5 lpm and it was operated at different supersaturations for each particle size in the range between 0.03 and 1%. The activated fraction was determined from the ratio between the CPC and CCN counts and the critical supersaturation was estimated as the supersaturation at which 50% of the particles were activated.

Deliquescence curves of 100 nm dry diameter particles were measured by means of a Hygroscopicity Tandem Differential Mobility Analyzer (H-TDMA) in order to analyse the aerosol hygroscopicity. The H-TDMA instrument used in this work consists of a bipolar neutraliser, a diffusion dryer, a fixed voltage long column DMA that is used to select a narrow size range of ambient aerosol, a humidification system, a second DMA used to determine the growth of the particles selected by the first DMA and a TSI 3760 CPC counter (Cubison et al., 2005; Gysel et al., 2009). A humidity below 10% RH was used for particle size selection in the first DMA. The DMAs used were of the Vienna design with a central column length of 0.28 m and a sheath flow rate of 6 lpm. The experimental set-up for the aerosol characterization is depicted in Fig. 1c, utilising the plunging-water jet as aerosol generation system. The sampling system for the other bubble-bursting systems was identical.

2.4.1 Particles morphology considerations

The shape and morphology of aerosol particles are relevant characteristics which might affect the aerosols sizing methods, through their effects on particle drag and transport properties. Particle size selection in DMA columns is based on the mobility diameter (d_m), which is dependent on the particle shape. For spherical particles mobility diameter is equivalent to volume diameter (d_{ve}); however for non-spherical particles this is not the case.

The shape of the particles depends on their chemical composition and generation mechanism. Different type of compounds may form particles of diverse morphology and aerosol particles containing the same compounds could exhibit different structure

and shape, depending on differences in particle generation (Rissman et al., 2007). The shape of the formed particles might also depend on the temperature range, the drying process and the addition of surfactants (Iskandar et al., 2003).

For cubic particles, such as NaCl, a standard shape factor of $\chi=1.08$ is generally applied in order to reconcile the mobility and volume equivalent diameters. This correction is necessary to estimate the particles hygroscopic growth and the volume equivalent diameter, usually employed as input parameter for calculations based on the Köhler theory. Although NaCl is an important component in both the artificial and natural seawater samples used in this work, it is likely that the presence of organics and other inorganic salts and the use of diverse generation mechanisms may lead to morphologies different to that of pure NaCl particles. Transmission Electron Microscope images of particles generated from artificial and natural seawater by bubble bursting have shown that the morphology of these particles differs from the well-known cubic shape of NaCl particles (Wise et al., 2009). In order to account for the uncertainty in the morphology of the particles produced by the different generators employed in this work, correction factors in the range from spherical ($\chi=1$) to cubic shape ($\chi=1.08$) are applied, with the averaged data evaluated with a factor of $\chi=1.04$.

3 Results

3.1 Bubble-bursting generators: bubble spectrum

Investigations on the study of the number and size of sea salt drops ejected by individual bubbles have demonstrated that the relative contribution of jet and film drops to the aerosol production depends critically on the characteristics of the parent bubble size distribution (Spiel, 1997; Wu, 2002). Laboratory reproduction of the oceanic bubble spectrum would therefore be relevant for the generation of a representative marine aerosol. In order to test the ability of the selected bubble-bursting methods for simulating the real oceanic bubble spectrum, the size distribution of the bubbles generated in

Laboratory-generated primary marine aerosol

E. Fuentes et al.

Title Page

Abstract

Introduction

Conclusions

References

Tables

Figures



Back

Close

Full Screen / Esc

Printer-friendly Version

Interactive Discussion



artificial seawater was experimentally determined.

The bubble spectrum produced by the aeration systems tested in this work are shown in Fig. 2. A bimodal distribution characterized by a narrow peak at 30–40 μm bubble diameter and a second broad mode between 200 and 300 μm was generated by the aquarium diffuser, while a multimodal spectrum was obtained for the glass sintered filter. Different sensitivity to the airflow was also observed for these two systems, with the glass frit spectrum exhibiting more variability to changes in the aeration flow. A common characteristic of these aeration distributions is that they present a large number of bubbles above 100 μm , which is agreement with previous observations of aerator spectrum made by Mårtensson et al. (2003) and Leifer et al. (2003). The bubble size distribution obtained for the water recirculation system, illustrated in Fig. 3, is characterized by a peak within the 40–80 μm diameter range followed by a less pronounced mode at 400–600 μm . The use of increasing water recirculation flow rates caused an increase in the bubble number within the whole size range as a result of a higher air entrainment in the water bulk, however the shape of the distribution was preserved. The differences in the shape of the bubble spectrum generated by the diverse systems indicate that different particle production rates and size distributions should be expected from the several aerosol generators used.

A number of observations of oceanic bubble spectrum, along with the experiments from the bubbling systems obtained in this work are illustrated in Fig. 4. Oceanic bubble measurements typically peak in a range from 40 to 80 μm diameter, with the bubble number decreasing with size from the peak concentration following a power-law scaling as a function of the bubble diameter, with an exponent which varies between 0.8 and 5 (Sellegrì et al., 2006; Deane and Stokes, 2002). The existence of a second peak at 400–600 μm has also been reported in oceanic spectrum in open ocean (de Leeuw and Cohen, 2002). The comparison presented in Fig. 4 indicates that the bubble distribution generated with the plunging-water jet system is most consistent with the oceanic measurements, since the typical shape of the real distribution is closely resembled.

The oceanic bubble spectrum power-law scaling has been proven to be related to

Laboratory-generated primary marine aerosol

E. Fuentes et al.

Title Page

Abstract

Introduction

Conclusions

References

Tables

Figures



Back

Close

Full Screen / Esc

Printer-friendly Version

Interactive Discussion



Laboratory-generated primary marine aerosol

E. Fuentes et al.

Title Page

Abstract

Introduction

Conclusions

References

Tables

Figures

◀

▶

◀

▶

Back

Close

Full Screen / Esc

Printer-friendly Version

Interactive Discussion



the life cycle of bubbles generated by breaking waves (Deane and Stokes, 2002). The lifetime of wave-generated bubbles is divided into two phases. The first stage takes place as the fluid jet is entrained in the water, and is known as the acoustically active phase. Once bubble production is finished, the formed bubble plume becomes acoustically quiescent and it evolves under the effect of turbulent diffusion, advection, buoyant degassing and dissolution (Deane and Stokes, 2002). Deane and Stokes (2002) studied the evolution of bubble plumes below whitecaps after breaking wave events. They reported an increasing value of the bubble spectrum power-law scaling exponent with time due to the bubble plume transition from the acoustic to the quiescent state. Oceanic measurements below breaking waves at the acoustic stage present a higher number of large bubbles than measurements under quiescent conditions, with power law exponents ranging from 0.8 to 1.9 (Deane and Stokes, 2002). On the other hand, oceanic measurements in quiescent plumes which had evolved from initial acoustic primary plumes present higher power scaling law exponents with values from 2.5 to 5.

The spatial distribution of the bubble population in the plunging-water jet system was characterised by measuring the bubble spectrum at different positions in the tank. Fields of bubble number and mean bubble size obtained from this analysis are depicted in Fig. 5a. Most of the bubble population and the large bubbles appear to be concentrated at the impingement region, while the bubble number and mean size are reduced as the sampling point is displaced from the plunging area. Figure 5b shows the spectrum of bubble plumes at different distances from the impinging point. A reduction in the number of bubbles with size above $100\ \mu\text{m}$ and a shift of the peak of the distribution to smaller sizes are observed as the distance from the water jet is increased. These trends account for the reduction in the number and size observed in the bubble spectrum field data in Fig. 5a. In these measurements the power-law exponent increases gradually as the sampling point is displaced from the impingement region, with a value of 1.49, to 4.5 at 110 mm from the tank centre. The value of the power-law exponent at the impingement area is in good agreement with observations from oceanic bubble formation regions (Deane and Stokes, 2002). Likewise, the power-law exponent

of the bubble spectrum obtained at 110 mm from the impinging zone is comparable to those of bubble spectrum measured in oceanic quiescent plumes, as was illustrated in Fig. 4. Similar gradual increase of the spectrum power-law exponent of acoustic bubble plumes evolving to quiescent state was observed by Deane and Stokes in their study of plumes formed at breaking wave events. These correspondences indicate that the bubble spectrum created below the plunging-water jet represents a bubble plume in the acoustic stage, in which a continuous generation of bubbles occurs, whilst measurements outside the plunging area correspond to bubble populations originated from a nascent bubble plume which has gradually evolved from acoustic to quiescent conditions.

3.2 Aerosol size distribution

Dry aerosol size distributions obtained from artificial seawater by using the different generation techniques are shown in Fig. 6. As the order of magnitude of particle production in the systems studied is considerably different, the results have been normalized to the total particle number for comparison purposes.

For a more accurate comparison of these multimodal size distributions each spectrum was decomposed into an optimum number of lognormal modes, so that the total size distribution is the result of the sum of the different modes. Four modes were found in the size distributions generated by using the bubble-bursting techniques, while only two modes comprise the distribution of the atomized aerosol. The properties of the measured size distributions are summarized in Table 1. The submicron particle size distribution generated by the plunging-water jet system presents modes at 15.3, 48, 131 and 341 nm. The second to fourth lognormal modes in the aeration-generated aerosol distributions peak at smaller sizes than those of the plunging-water jet aerosol, whereas only the glass sintered filter measurement shows a significant mode at 340 nm. A foam of pseudo-stable bubbles, which only exists when bubbling with the glass sintered filter and the plunging-water jet might be related to the formation of this fourth mode of larger particles. Furthermore, the higher significance of the

Laboratory-generated primary marine aerosol

E. Fuentes et al.

Title Page

Abstract

Introduction

Conclusions

References

Tables

Figures



Back

Close

Full Screen / Esc

Printer-friendly Version

Interactive Discussion



fourth lognormal mode in the plunging-water jet measurement with respect to the distributions derived from the aeration techniques seems to be associated to a mechanism predominant in the plunging-jet system, probably related to the formation of particles from droplet splashing which occurs at the impact of the liquid jet on the water surface.

5 Sellegri et al. (2006) found that the size distributions obtained by using a weir system and glass frits of different porosity presented a pattern characterized by a dominant peak at around 100 nm and a secondary mode at 350 nm, more significant in the weir system. Splashing is stronger in our plunging-water jet generator than in the referred authors' weir system, which explains that the largest fourth mode of the plunging-water
10 jet distribution is very significant in our experiments and that the size distribution from this generator differs considerably from the distributions generated using the aerators. Furthermore, the size distributions are consistent with the bubble spectrum measurements presented above, since in the aerators spectrum the number of large bubbles is higher than in the plunging-water jet spectrum (water flow 0.8 lpm) and large bubbles
15 are associated to the production of a high number of small film droplets.

As the first three lognormal modes are substantial in all the bubbling experiments they should all be mainly related to bubble bursting. Although it is not clear the occurrence of different modes could be associated to diverse bubble bursting scales, the multimodal character of the bubble spectrum obtained for these systems could be responsible for the formation of multimodal aerosol distributions. Furthermore, according
20 to Leifer et al. (2003), in addition to bubble formation through air entrainment by breaking waves, bursting of initial bubbles can form clouds of secondary bubbles near the water surface. The bursting of these groups of secondary bubbles in addition to the bursting of the primary bubbles might contribute to the formation of the different modes
25 comprising these particle size distributions.

Figure 7 shows the size distributions obtained in this study along with a submicron oceanic particle size distribution obtained at the Mace Head atmospheric research station by Sellegri et al. (2006). The oceanic distribution was measured in a month with low biological activity (January 2004), thus a low organic content is expected in these

Laboratory-generated primary marine aerosol

E. Fuentes et al.

Title Page

Abstract

Introduction

Conclusions

References

Tables

Figures



Back

Close

Full Screen / Esc

Printer-friendly Version

Interactive Discussion



oceanic waters and it should be comparable with our measurements obtained using organics-free artificial seawater. Decomposition of the oceanic measurement into log-normal modes showed that the real size distribution also comprised four modes. In this size distribution the fourth lognormal mode is more dominant than in the aeration techniques measurements but not as significant as in the plunging-water jet distribution. This indicates that in the real sea spray there might be an important contribution from particles generated from splashing and foam formation; however, the magnitude of this lognormal mode is expected to depend on the intensity of wave breaking.

Figure 7b indicates that, generally, the shape of the real size distribution is closely resembled by the plunging-water jet system, although the individual modes of the real size distribution present modal sizes which are 31 to 70% smaller than those in the laboratory experiments. This discrepancy is expected since our measurements were conducted at 20°C while the field data corresponds to seawater at 4°C and it has been proven that a decrease in the water temperature leads to a reduction in the size of the emitted particles (Sellegrì et al., 2006).

3.3 Hygroscopicity and CCN activity

Artificial seawater samples free of organics were used to study the hygroscopicity of aerosols generated by the different techniques on study. Hygroscopic growth in the humidity range from 50 to 93% RH was measured for 100 nm dry diameter particles. Figure 8a shows the hydration behaviour of particles produced from artificial seawater using the different aerosol generation techniques, along with experimental and theoretical data for pure NaCl.

The error bars on the plunging-waterjet curve result from the uncertainty in the diameter selected by the DMA, calculated considering correction factors in the range from spherical ($\chi=1$) to cubic shape ($\chi=1.08$), whereas the presented data corresponds to a shape factor of $\chi=1.04$. Although not included here for clarity, the same uncertainty range should be considered for all the seawater experiments.

Without significant differences between the studied cases, observable water uptake

Title Page

Abstract

Introduction

Conclusions

References

Tables

Figures



Back

Close

Full Screen / Esc

Printer-friendly Version

Interactive Discussion



5 already occurred at 50% humidity, followed by a progressive growth with increasing RH and a substantial water uptake in the 70 to 80% humidity range. The characteristics of this humidogram are in agreement with observations of ambient marine aerosols (Winkler et al., 1972; Tang et al., 1997) and aerosols generated from artificial and natural
10 seawater samples (Cziczo et al., 1997; Wise et al., 2009). The hygroscopic properties of sea salt particles are consistent with what is expected from a multicomponent aerosol system. The presence of salts of low deliquescence point, such as $MgCl_2$, are considered to be responsible for the water uptake occurring at RH lower than that of NaCl (Cziczo et al., 1997), while the significant growth at around 75% RH is associated
15 to the total dissolution of NaCl crystals.

Seawater proxies with organics of biogenic origin at $DOC\ 512\ \mu M$ were prepared to compare the behaviour of particles produced by the different aerosol generators. Figure 8b presents the hygroscopic growth of the particles generated from seawater proxies containing *Thalassiosira rotula* algal exudate along with the theoretical and experimental curves for NaCl. The existence of organic material in the sea-salt particles
20 suppresses the hygroscopic growth in comparison with the artificial seawater measurements in all the cases, although the magnitude of the observed effects is dependent on the generation technique employed. The main differences between the humidograms are observed above 75% RH, with the plunging-water jet presenting the highest growth suppression. The rest of cases show a similar behaviour up to 87% RH, point
25 above which the humidograms for the aerators and the nebulizer diverge. Wise et al. (2009) reported analogous findings to our results in their comparison of the morphological changes of growing sea salt particles generated from artificial and natural seawater using two different aerosol generators. These authors found that there were no differences in the hygroscopic properties of organics-free artificial seawater particles generated by either atomization or foam-bubble bursting; however, they observed a difference in the onset of morphological changes and rounding of particles generated from natural seawater when using the two methods for particle production.

The CCN activity of particles generated from artificial seawater and seawater con-

Laboratory-generated primary marine aerosolE. Fuentes et al.

[Title Page](#)[Abstract](#)[Introduction](#)[Conclusions](#)[References](#)[Tables](#)[Figures](#)[◀](#)[▶](#)[◀](#)[▶](#)[Back](#)[Close](#)[Full Screen / Esc](#)[Printer-friendly Version](#)[Interactive Discussion](#)

taining biogenic organic solutions was characterized for dry particle diameters between 40 and 110 nm. Critical supersaturations obtained from these experiments are shown in Fig. 9a–c, along with the theoretical curve for NaCl. The horizontal error bars account for the uncertainty in the selection of the particle diameter by the DMA in the range from spherical ($\chi=1$) to cubic ($\chi=1.08$) particle shape, and the vertical error bars indicate the uncertainty in the determination of the critical supersaturation taken as $\pm 1\sigma$ standard deviation. Although not included in all the cases in Fig. 9a–c for clarity of presentation, the same uncertainty range should be considered in all the experiments.

Whereas the measurements with artificial seawater indicate no significant effects on the critical supersaturation with respect to the theoretical values for NaCl, the presence of biogenic organics caused an increase in the critical supersaturation in all the cases; however, the degree of this effect is dependent on the aerosol generation system. Percent variations presented in Fig. 9d show a large effect for the atomization experiments, with a notable increase in the critical supersaturation with increasing particle size from 6% at 38 nm (d_{ve}) to 43.8% at 96.3 nm (d_{ve}), with respect to the case without organics. This behaviour suggests the occurrence of organic component size fractionation in the particles generated from atomization. More similar magnitude of this influence is observed for the bubbling-bursting methods, with a 17% averaged increase in the critical supersaturation for the plunging water jet and a lower influence for the aerators (11%). However, a homogeneous effect is observed with respect to the particle size for these systems. Although the presence of surface-active organic material in the particles would induce a reduction in the surface tension and, consequently, a decrease in the critical supersaturation according to the equilibrium Köhler theory, the observed increase in the critical supersaturation might be due to a dominance of the Raoult term because of the replacement of inorganic salts by organic compounds and surface to bulk partitioning effects (Li et al., 1998; Sorjamaa et al., 2004). A detailed analysis of the influence of the marine biopolymers on the particles CCN behaviour is beyond the scope of this work and will be presented elsewhere. Nevertheless, it is clear that representative bubble-bursting and aerosol generation mechanisms must be used to

Laboratory-generated primary marine aerosol

E. Fuentes et al.

Title Page

Abstract

Introduction

Conclusions

References

Tables

Figures

◀

▶

◀

▶

Back

Close

Full Screen / Esc

Printer-friendly Version

Interactive Discussion



simulate these effects.

The discrepancies in the hygroscopicity and CCN activity of aerosols generated by the different systems indicate that the mechanism producing the particles influences their organics enrichment. The presence of organics on sea salt particles generated by bubble-bursting is due to organic matter which partitions to the air-water interface of the bubbles during ascent. The sea-water-to air transfer of surface active organic compounds has been demonstrated to be closely related to the bubble scavenging process, which is critically dependent on the bubble spectrum and the chemical properties of the material being absorbed by the bubbles (Tseng et al., 1992). Although the aerosol bubble-bursting methods are mechanistically analogous from the viewpoint of aerosol generation, their different bubble formation processes might affect the organics scavenging by bubbles during its existence in the water bulk, and so affect the aerosol organic enrichment. The bubbles residence time is a factor controlling the absorption of organics on the bubbles interface since the scavenging of organics by bubbles generated in an organics solution has been proven to be strongly dependent on the bubble rise distance (Blanchard, 1964). In the plunging-water jet system the bubbles reach their terminal velocity rapidly after the plume formation, as determined by the balance between buoyancy and drag forces. An important factor in bubble hydrodynamics is the presence of surfactants, which can partially immobilize the surface, increasing drag and decreasing rise velocity. Assuming the bubbles generated by the plunging-water jet system are isolated bubbles whose surface is saturated with surfactants, their rising terminal velocity can be described by (Batchelor, 1967):

$$U_0^2 = \frac{4}{3} \frac{d(\rho - \rho_g)}{\rho C_{d0}} \quad (1)$$

$$C_{d0} = \frac{12}{\text{Re}_0} (1 + 0.104\text{Re}_0) , \quad (2)$$

where U_0 is the terminal rising velocity of the bubbles, ρ is the density of the liquid, ρ_g is the air density, C_{d0} is the drag coefficient and Re_0 is the Reynolds number.

Laboratory-generated primary marine aerosol

E. Fuentes et al.

Title Page

Abstract

Introduction

Conclusions

References

Tables

Figures

◀

▶

◀

▶

Back

Close

Full Screen / Esc

Printer-friendly Version

Interactive Discussion



The rise velocity of bubbles formed via aeration is additionally affected by the in-line hydrodynamic interaction between bubbles, which generates an upwelling flow which in turn causes the trailing bubbles to rise faster than single bubbles in still water. This is the so-called wake effect. The ratio between the rise velocity of a trailing bubble generated by aeration U_{aer} and the rising velocity of an isolated bubble U_0 is given by (Zhang and Fan, 2003):

$$U_{\text{aer}}/U_0 = 1 + \frac{C_{\text{d0}}}{2} \left[1 - \exp\left(\frac{\text{Re}_0}{x/D_b}\right) \right], \quad (3)$$

where x is the distance between the trailing bubbles and D_b is the bubble diameter. The distance between the bubbles is determined by the number of bubbles in the rising column, which depends on the air flow through the porous media:

$$x = \frac{h(1 - D_b N_b)}{N_b - 1} \quad (4)$$

$$N_b = \frac{Q_p}{V_b U_{\text{aer}}}, \quad (5)$$

where Q_p is the air flow per pore, N_b is the number of bubbles per cm and h is the distance from the porous unit where the bubbles are generated to the water surface.

Figure 10 (left axis, U_{aer}/U_0) shows the ratio between the terminal velocity of bubbles generated with the glass sintered filter (U_{aer}) and the bubbles generated with the plunging-water jet system (U_0), calculated using Eqs. (1–3) for two different air flows through the glass frit. The rise velocity of the glass frit interactive bubbles is higher than that of the bubbles generated by the plunging-water jet system for bubble sizes below $140 \mu\text{m}$. This difference is due to the wake effect, which is responsible for the acceleration of the bubbles generated by aeration and is enhanced by increasing flow rates. As the bubble size is increased, the rising velocity of the bubbles produced by both techniques is equal because buoyancy becomes the dominant force in the motion of large size bubbles.

[Title Page](#)
[Abstract](#)
[Introduction](#)
[Conclusions](#)
[References](#)
[Tables](#)
[Figures](#)
[◀](#)
[▶](#)
[◀](#)
[▶](#)
[Back](#)
[Close](#)
[Full Screen / Esc](#)
[Printer-friendly Version](#)
[Interactive Discussion](#)


Laboratory-generated primary marine aerosol

E. Fuentes et al.

Title Page

Abstract

Introduction

Conclusions

References

Tables

Figures

◀

▶

◀

▶

Back

Close

Full Screen / Esc

Printer-friendly Version

Interactive Discussion



Figure 10 (right axis, t_{aer}/t_0) shows the residence time ratio of bubbles generated by the aeration method (t_{aer}) with respect to the plunging-water jet bubbles (t_0). The residence times were calculated taking into account path lengths of 10 and 5 cm for the plunging-water jet and the glass frit, respectively. The rising distance for the plunging-water jet is the plume penetration distance and the glass sintered filter distance is determined by the filter position below the water surface. The residence time of bubbles produced by the glass sintered filter is significantly less than that of the plunging-water jet bubbles in a ratio ranging from 0.55 to 0.87 at a flow of 5 lpm. This difference is enhanced for bubble sizes below $140 \mu\text{m}$, the range in which the wake effect is significant, especially for the highest air flow case. Above $140 \mu\text{m}$ the dissimilar residence times are due to the different rising distance in the two systems, as the rise velocity of the bubbles produced by both generators was shown to be identical.

The bubble spectrums corresponding to the glass frit and the plunging-water jet represented in Fig. 10 indicate that the largest difference in the bubbles lifetime for these two systems occurs in the range of bubble spectrum below $140 \mu\text{m}$, where 80–90% of the bubble population is found. As the bubbles of small size are considered to be more effective in the scavenging of surfactants than large size bubbles due to their longer life in the water bulk, it is expected that a lower organic enrichment will occur in bubbles generated by the glass frit. This eventually might lead to a lower organics enrichment of the formed particles, explaining the reduced effects observed in the suppression of growth factors and the impact on the critical supersaturation for the aeration experiments with respect to the plunging-water jet measurements.

4 Summary and conclusions

Different laboratory aerosol generation techniques were tested in order to assess their validity for artificially producing marine aerosol in laboratory studies. Two aeration methods and a plunging-water jet system were tested as bubble-bursting aerosol generators for comparison with a standard nebulizer. The systems for aerosol production were

evaluated by analysing the bubble spectrum generated by the bubble-bursting methods and the size distribution, hygroscopicity and CCN activity of the aerosols generated by the different techniques.

The bubble spectrum obtained with the plunging-water jet system resembled the real oceanic spectrum with a dominant peak at 20–40 μm and a typical oceanic power-law scaling profile with exponents ranging from 1.4 to 4.5. Comparison of the power-law exponents with real spectrum measurements near bubble formation indicated that the nascent plume generated by the plunging-water jet mimics an acoustic bubble plume which evolves to a quiescent state as it is dispersed in the water bulk.

The multimodal aerosol size distributions obtained with the different generators were decomposed into single lognormal modes in order to compare and identify the different mechanisms contributing to the formation of the aerosol. Three bubble-bursting related modes and one foam/splashing related mode were found in the bubble-bursting techniques distributions, whereas only two modes comprised the atomizer particle size distribution. The aeration distributions presented a peak at smaller sizes and higher particle number than that of the plunging-water jet. These results are consistent with our bubble spectrum measurements, since a larger number of bubbles above 100 μm is produced by the aerators and large bubbles produce a higher number of small film drops. Comparisons made with a marine aerosol size distribution atmospheric measurement (Sellegrì et al., 2006) indicated the plunging-water jet system reproduces the real distribution signature most closely.

Hygroscopic growth of particles generated from artificial seawater occurred at lower relative humidities than that of NaCl, but similar growth to the pure salt was obtained above 75% RH. No observable differences were found between the behaviour of the aerosol generated from artificial seawater by the different techniques. Hygroscopic growth was suppressed with respect to the organics-free artificial seawater experiments when the aerosol was generated from a seawater proxy with biogenic surfactants, although the extent of this reduction was dependent on the aerosol generation technique applied.

Laboratory-generated primary marine aerosol

E. Fuentes et al.

Title Page

Abstract

Introduction

Conclusions

References

Tables

Figures



Back

Close

Full Screen / Esc

Printer-friendly Version

Interactive Discussion



Laboratory-generated primary marine aerosol

E. Fuentes et al.

Title Page

Abstract

Introduction

Conclusions

References

Tables

Figures

◀

▶

◀

▶

Back

Close

Full Screen / Esc

Printer-friendly Version

Interactive Discussion



Likewise, the CCN activity of particles generated from artificial seawater did not show observable differences with respect to that of pure NaCl when using the different techniques. However, the use of seawater with biogenic organics in the parent solution produced an increase in the critical supersaturation with respect to the case without organics. The extent of this effect was dependent on the aerosol generator employed. A large effect was observed for the atomization experiments, with a notable increment in the critical supersaturation with increasing particle size with respect to the case without organics. Reduced effects were observed for the bubbling-bursting methods, with a 17% increase for the plunging-water jet and 11% for the aerators, without any size fractionation effect.

The hygroscopicity and CCN measurements in this work suggest that the aerosol generation mechanism affects the particles organic enrichment, thus the behaviour of the produced aerosols strongly depends on the laboratory aerosol generator employed. Calculations of rising speed of surfactants-enriched bubbles generated by the glass sintered filter and the plunging-water jet showed that the residence time of the bubbles created by aeration was lower than that of the plunging-water jet bubbles in a ratio from 0.55 to 0.87. This discrepancy was larger for increasing air flows through the aerator, due to wake effects on bubbles with diameters below 140 μm . The shorter life of small bubbles might reduce the amount of surfactants scavenged by the bubbles and hence, the organic matter enrichment of the generated particles. This would explain that reduced effects in the growth factor and critical supersaturation were observed for the aerator compared to the plunging-water jet particles.

The results of this work have demonstrated that different mechanisms for aerosol production in the laboratory lead to diverging experimental results in the aerosol behaviour. Consensus in the use of a proper marine aerosol generator for these types of studies is therefore relevant to make laboratory experiments representative of real atmospheric processes. According to this study, a generator consisting of a plunging-water jet is able to produce bubble populations and aerosol size distributions that resemble the real bubble and aerosol distributions signatures. A system demonstrating

these characteristics is expected to generate particles whose behaviour is more representative of primary marine aerosols compared to other laboratory generators.

Acknowledgements. This work was supported by the UK Natural Environment Research Council [grant numbers NE/D005175/1 and NE/G000247/1]. The authors would like to thank Dr. G. de Leeuw and L. H. Cohen from the Netherlands Organisation for Applied Scientific Research (TNO) for their cooperation and assistance in the use of the BMS instrument.

References

- Aluwihare, L. I. and Repeta, D. J.: A comparison of the chemical characteristics of oceanic DOM and extracellular DOM produced by marine algae, *Mar. Ecol. Prog. Ser.*, 186, 105–117, 1999. 2284
- Batchelor, G. K.: *An Introduction to Fluid Dynamics*, Cambridge University Press, Cambridge, 1967. 2300
- Blanchard, D. C.: Sea-to-air transport of surface active material, *Science*, 146, 396–397, 1964. 2300
- Boehme, J., Frisches, M. E., Jiang, S. C., Kellog, C. A., Pichard, S., Rose, J. B., Steinway, C., and Paul, J. H.: Viruses, bacterioplankton, and phytoplankton in the southeastern Gulf of Mexico: distribution and contribution to oceanic DNA pools, *Mar. Ecol. Prog. Ser.*, 97, 1–10, 1993. 2283
- Braban, C.F., Adams, J. W., Rodriguez, D., Cox, R. E., Crowley, J. N., and Schuster, G.: Heterogeneous reactions of HOI, ICl and IBr on sea salt and sea salt proxies, *Phys. Chem. Chem. Phys.*, 9, 3136–3148, 2007. 2284, 2285
- Cipriano R. J. and Blanchard, D.: Bubble and Aerosol Spectra Produced by a Laboratory “Breaking Wave”, *J. Geophys. Res.*, 86(C9), 8085–8092, 1981. 2284
- Cloke, J., McKay, W. A., and Liss, P. S.: Laboratory investigations into the effect of marine organic material on the sea-salt aerosol generated by bubble bursting, *Mar. Chem.*, 34, 77–95, 1991. 2284
- Cziczo, D. J., Nowak, J. B., Hu, J. H., and Abbatt, J. P. D.: Infrared spectroscopy of model tropospheric aerosols as a function of relative humidity: Observation of deliquescence and crystallization, *J. Geophys. Res.*, 102, 18843–18850, 1997. 2298

Laboratory-generated primary marine aerosol

E. Fuentes et al.

Title Page

Abstract

Introduction

Conclusions

References

Tables

Figures

◀

▶

◀

▶

Back

Close

Full Screen / Esc

Printer-friendly Version

Interactive Discussion



Laboratory-generated primary marine aerosol

E. Fuentes et al.

[Title Page](#)[Abstract](#)[Introduction](#)[Conclusions](#)[References](#)[Tables](#)[Figures](#)[◀](#)[▶](#)[◀](#)[▶](#)[Back](#)[Close](#)[Full Screen / Esc](#)[Printer-friendly Version](#)[Interactive Discussion](#)

- Cubison, M. J., Coe, H., and Gysel, M.: A modified hygroscopic tandem DMA and a data retrieval method based on optimal estimation, *J. Aerosol. Sci.*, 36, 846–865, 2005. 2291
- de Leeuw, G. and Cohen, L. H.: Bubble size distributions on the North atlantic and North Sea, *Geophysical monograph, Am. Geo. Union*, 127, 271–277, 2002. 2293, 2314
- 5 Deane, G. B. and Stokes, M. D.: Scale dependence of bubble creation mechanisms in breaking waves, *Nature*, 418, 839–844, 2002. 2293, 2294
- Duce, R. A. and Hoffman, E. J.: Chemical fractionation at the air/sea interface, *Annu. Rev. Earth Planet. Sci.*, 4, 187–228, 1976. 2284
- Facchini, M. C., Rinaldi, M., Decesari, S., Carbone, C., Finessi, E., Mircea, M., Fuzzi, S., Ceburnis, D., Flanagan, R., Nilsson, E.D., de Leeuw, G., Martino, M., Woeltjen, J., and O'Dowd, C. D.: Primary submicron marine aerosol dominated by insoluble organic colloids and aggregates, *Geophys. Res. Lett.*, 35, L17814, doi:10.1029/2008GL034210, 2008. 2284
- 10 Fitzgerald, J. W.: Marine aerosols: a review, *Atmos. Environ.*, 25A, 533–546, 1991. 2283
- Guillard, R. R. L.: Culture of phytoplankton for feeding marine invertebrates, in: *Culture of Marine Invertebrate Animals*, edited by: Smith, W. L. and Chanley, M. H., Plenum Press, New York, 26–60, 1975.
- 15 Gysel, M., McFiggans, G. B., and Coe, H.: Inversion of tandem differential mobility analyser (TDMA) measurements, *J. Aerosol Sci.*, 40, 134–151, 2009. 2291
- Iskandar, F., Gradon, L., and Okuyama, K.: Control of the morphology of nanostructured particles prepared by the spray drying of a nonparticle sol, *J. Col. Interf. Sci.*, 265, 396–303, 2003. 2292
- 20 Keene, W. C., Maring, H., Maben, J. R., Kieber, D. J., Pszenny, A. A. P., Dahl, E. E., Iza-guirre, M. A., Davis, A. J., Long, M. S., Zhou, X., Smoydzin L., and Sander, R.: Chemical and physical characteristics of nascent aerosols produced by bursting bubbles at a model air-sea interface, *J. Geophys. Res.*, 112, D21202, doi:10.1029/2007JD008464, 2007. 2284
- 25 Kester, D. R., Duedall, I. W., Connors, D. N., and Pytkowicz, R. M.: Preparation of artificial seawater, *Limnol. Oceanogr.*, 12, 176–179, 1967. 2288
- Leifer, I., de Leeuw, G., and Cohen, L. H.: Optical measurement of bubbles: system design and application, *J. Atmos. Ocean. Tech.*, 20, 1317–1332, 2003. 2290, 2293, 2296
- 30 Leifer, I., de Leeuw, G., and Cohen, L. H.: Secondary bubble production from breaking waves: The bubble burst mechanism, *Geophys. Res. Lett.*, 27, 4077–4080, 2000.
- Li, Z., Williams, A. L., and Rood, M. J.: Influence of soluble surfactant properties on the activation of aerosol particles containing inorganic solute, *J. Atmos. Sci.*, 55, 1859–1866, 1998.

- Mårtensson, E. M., Nilsson, E. D., Cohen, L. H., and de Leeuw, G.: Laboratory simulations and parameterization of the primary marine aerosol production, *J. Geophys. Res.*, 108(D9), 4297, doi:10.1029/2002JD002263, 2003. 2284, 2285, 2293
- 5 McFiggans, G., Artaxo, P., Baltensperger, U., Coe, H., Facchini, M. C., Feingold, G., Fuzzi, S., Gysel, M., Laaksonen, A., Lohmann, U., Mentel, T. F., Murphy, D. M., O'Dowd, C. D., Snider, J. R., and Weingartner, E.: The effect of physical and chemical aerosol properties on warm cloud droplet activation, *Atmos. Chem. Phys.*, 6, 2593–2649, 2006, <http://www.atmos-chem-phys.net/6/2593/2006/>. 2284
- 10 McNeill, V. F., Patterson, J., Wolfe, G. M., and Thornton, J. A.: The effect of varying levels of surfactant on the reactive uptake of N₂O₅ to aqueous aerosol, *Atmos. Chem. Phys.*, 6, 1635–1644, 2006, <http://www.atmos-chem-phys.net/6/1635/2006/>. 2284, 2285
- Niedermeier, D., Wex, H., Voigtländer, J., Stratmann, F., Brüggemann, E., Kiselev, A., Henk, H., and Heintzenberg, J.: LACIS-measurements and parameterization of sea-salt particle hygroscopic growth and activation, *Atmos. Chem. Phys.*, 8, 579–590, 2008, <http://www.atmos-chem-phys.net/8/579/2008/>. 2284, 2285
- O'Dowd, C. D., Smith, M. H., Consterdine, I. E., and Lowe, J. A. : Marine aerosol, sea-salt, and the marine sulphur cycle: a short review, *Atmos. Environ.*, 31, 73–80, 1997. 2283
- 20 O'Dowd, C. D., Facchini, M. C., Cavalli, F., Ceburnis, D., Mircea, M., Decesari, S., Fuzzi, S., Yoon, Y. J., and Putaud, J.-P.: Biogenically driven organic contribution to marine aerosol, *Nature*, 431(7009), 676–680, 2004. 2283, 2286
- O'Dowd, C. D. and de Leeuw, G.: Marine aerosol production: a review of the current knowledge, *Philos. T. Roy. Soc.*, 365, 2007–2043, 2007. 2283, 2286
- 25 Ramaswamy, V., Boucher, O., Haigh, J., Hauglustaine, D., Haywood, J., Myhre, G., Nakajima, T., Shi, G. Y., and Solomon, S.: *Climate Change 2001: The Scientific Basis. Contribution of working group I to the Third Assessment Report of the Intergovernmental Panel on Climate Change*, 2001. 2283
- Rapp, R. J. and Melville, W. K.: Laboratory measurements of deep-water breaking waves, *Philos. T. Roy. Soc. London A*, 331, 735–800, 1990. 2283
- 30 Rissman, T. A., Varutbangkul, V., Surratt, J. D., Topping, D. O., McFiggans, G., Flagan, R. C., and Seinfeld, J. H.: Cloud condensation nucleus (CCN) behavior of organic aerosol particles generated by atomization of water and methanol solutions, *Atmos. Chem. Phys.*, 7, 2949–

Laboratory-generated primary marine aerosol

E. Fuentes et al.

Title Page

Abstract

Introduction

Conclusions

References

Tables

Figures

◀

▶

◀

▶

Back

Close

Full Screen / Esc

Printer-friendly Version

Interactive Discussion



2971, 2007,

<http://www.atmos-chem-phys.net/7/2949/2007/>. 2292

Riziq, A., Erlick, C., Dinar, E., and Rudich, Y.: Optical properties of absorbing and non-absorbing aerosols retrieved by cavity ring down (CRD) spectroscopy, *Atmos. Chem. Phys.*, 7, 1523–1536, 2007,

<http://www.atmos-chem-phys.net/7/1523/2007/>. 2284

Roberts, G. C. and Nenes, A.: A continuous-flow streamwise thermal-gradient CCN chamber for atmospheric measurements, *Aerosol Sci. Tech.*, 39, 206–221, 2005.

Saul, T. D., Tolocka, M. P., and Johnston, M. V.: Reactive uptake of nitric acid onto sodium chloride aerosols across a wide range of relative humidities, *J. Phys. Chem. A*, 110, 7614–7620, 2006. 2284, 2285

Sellegrì, K., O'Dowd, C. D., Yoon, Y.J., Jennings, S. G., and de Leeuw, G.: Surfactants and sub-micron sea spray generation, *J. Geophys. Res.*, 111, D22215, doi:10.1029/2005JD006658, 2006. 2284, 2285, 2293, 2296, 2297, 2303, 2310, 2317

Sorjamaa, R., Svenningsson, B., Raatikainen, T., Henning, S., Bilde, M., and Laaksonen, A.: The role of surfactants in Köhler theory reconsidered, *Atmos. Chem. Phys.*, 4, 2107–2117, 2004,

<http://www.atmos-chem-phys.net/4/2107/2004/>. 2299

Spiel, D. E.: A hypothesis concerning the peak in film drop formation as a function of bubble size, *J. Geophys. Res.*, 102, 1153–1161, 1997.

Stewart, D. J., Griffiths, P. T., and Cox, R. A.: Reactive uptake coefficients for heterogeneous reaction of N_2O_5 with submicron aerosols of NaCl and natural sea salt, *Atmos. Chem. Phys.*, 4, 1381–1388, 2004,

<http://www.atmos-chem-phys.net/4/1381/2004/>. 2284, 2285

Svenningsson, B., Rissler, J., Swietlicki, E., Mircea, M., Bilde, M., Facchini, M. C., Decesari, S., Fuzzi, S., Zhou, J., Mønster, J., and Rosenørn, T.: Hygroscopic growth and critical supersaturations for mixed aerosol particles of inorganic and organic compounds of atmospheric relevance, *Atmos. Chem. Phys.*, 6, 1937–1952, 2006,

<http://www.atmos-chem-phys.net/6/1937/2006/>. 2284, 2285

Taketani, F., Kanaya Y., and Akimoto, H.: Heterogeneous loss of HO_2 by KCl, synthetic sea salt, and natural seawater aerosol particles, *Atmos. Environ.*, 43, 1660–1665, 2009. 2284

Tang, I. N., Tridico, A. C., and Fung, K. H.: Thermodynamical and optical properties of sea salt aerosols, *J. Geophys. Res.*, 102, 23269–23275, 1997. 2298

Laboratory-generated primary marine aerosol

E. Fuentes et al.

Title Page

Abstract

Introduction

Conclusions

References

Tables

Figures

◀

▶

◀

▶

Back

Close

Full Screen / Esc

Printer-friendly Version

Interactive Discussion



Tseng, R., Viechnicki, J. T., Skop, R. A., and Brown, J. W.: Sea-to air transfer of surface active organic compounds by bubble bursting bubbles, *J. Geophys. Res.*, 97, 5201–5206, 1992. 2284, 2300

5 Tyree, C. A., Hellion, V. M., Alexandrova, O. A., and Allen, J. O.: Foam droplets generated from natural and artificial seawaters, *J. Geophys. Res.*, 112, D12204, doi:10.1029/2006JD007729, 2007. 2284, 2285

Vagle, S. and Farmer, D. M.: The measurement of bubble-size distributions by acoustical backscatter, *J. Atmos. Ocean. Tech.*, 9, 630–644, 1992. 2314

10 Williams, P. I.: Construction and validation of a DMPS for aerosol characterisation, University of Manchester, PhD Thesis, 1999. 2290

Williams, P. I., McFiggans, G., and Gallagher, M. W.: Latitudinal aerosol size distribution variation in the Eastern Atlantic Ocean measured aboard the FS-Polarstern, *Atmos. Chem. Phys.*, 7, 2563–2573, 2007, <http://www.atmos-chem-phys.net/7/2563/2007/>. 2290

15 Winkler, P. and Junge, C.: The growth of atmospheric aerosol particles as a function of the relative humidity, I, Methods and measurements at different locations, *J. Res. Atmos.*, 18, 617–638, 1972. 2298

20 Wise, M. E., Freney, E. J., Tyree, C. A., Allen, J. O., Martin, S. T., Russel, L. M., and Buseck, P. R.: Hygroscopic behaviour and liquid-layer composition of aerosol particles generated from natural and artificial seawater, *J. Geophys. Res.*, 114, D03201, doi:10.1029/2008JD010449, 2009. 2284, 2292, 2298

Wu, J.: Jet Drops Produced by Bubbles Bursting at the Surface of Seawater, *J. Phys. Ocean.*, 32, 3286–3290, 2002.

25 Zhang, J. and Fan, L.-S.: On the rise velocity of an interactive bubble in liquids, *Chem. Eng. J.*, 92, 169–176, 2003. 2301

Laboratory-generated primary marine aerosol

E. Fuentes et al.

Title Page

Abstract

Introduction

Conclusions

References

Tables

Figures

◀

▶

◀

▶

Back

Close

Full Screen / Esc

Printer-friendly Version

Interactive Discussion



Laboratory-generated primary marine aerosol

E. Fuentes et al.

Table 1. Characteristics of aerosol size distributions obtained from artificial seawater samples in this study in comparison with atmospheric marine aerosol measurements (Sellegrì et al., 2006) (dpg, geometric mean diameter; σ , geometric standard deviation; N/N_t (%), lognormal mode particle number to total number ratio).

	Mode 1			Mode 2			Mode 3			Mode 4		
	dpg (nm)	σ	N/N_t (%)									
Plunging-water jet	15.3	1.8	0.382	48	1.6	0.317	131	1.4	0.168	340	1.5	0.133
Glass sintered filter	20	1.7	0.089	41	1.5	0.452	90	1.8	0.417	253	1.2	0.041
Aquarium diffuser	12	1.9	0.130	40	1.8	0.50	90	1.7	0.348	300	1.4	0.015
Atomizer	36	1.6	0.530	100	1.9	0.462						
Field data (Sellegrì et al. 2006)	15	1.5	0.072	35	1.7	0.497	100	1.5	0.283	200	1.5	0.148

[Title Page](#)
[Abstract](#)
[Introduction](#)
[Conclusions](#)
[References](#)
[Tables](#)
[Figures](#)
[Back](#)
[Close](#)
[Full Screen / Esc](#)
[Printer-friendly Version](#)
[Interactive Discussion](#)


Laboratory-generated primary marine aerosol

E. Fuentes et al.

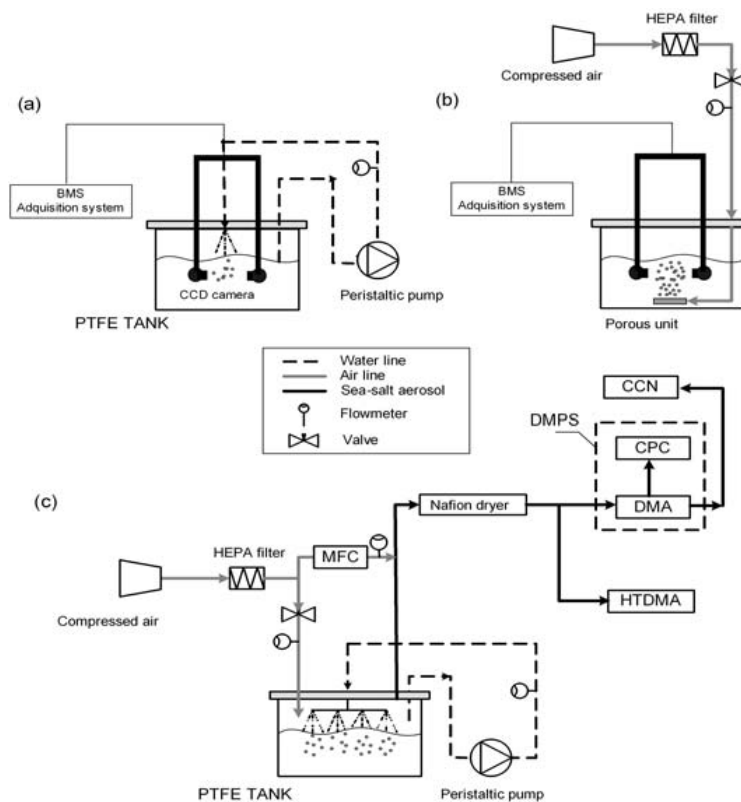


Fig. 1. Schematic of bubble spectrum experiments for **(a)** the plunging-water jet system and **(b)** the aeration methods. **(c)** Experimental set-up for aerosol size distribution, hygroscopicity and CCN experiments (the schematic represented corresponds to the plunging-water jet system).

Title Page

Abstract

Introduction

Conclusions

References

Tables

Figures

◀

▶

◀

▶

Back

Close

Full Screen / Esc

Printer-friendly Version

Interactive Discussion



Laboratory-generated primary marine aerosol

E. Fuentes et al.

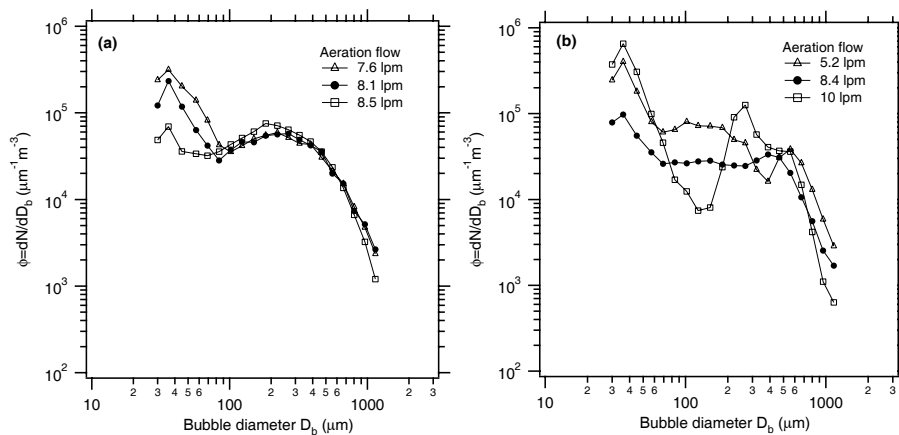


Fig. 2. Bubble population distribution versus bubble diameter for the plume generated by the (a) aquarium diffuser and (b) glass sintered filter at different aeration flows.

[Title Page](#)[Abstract](#)[Introduction](#)[Conclusions](#)[References](#)[Tables](#)[Figures](#)[◀](#)[▶](#)[◀](#)[▶](#)[Back](#)[Close](#)[Full Screen / Esc](#)[Printer-friendly Version](#)[Interactive Discussion](#)

Laboratory-generated primary marine aerosol

E. Fuentes et al.

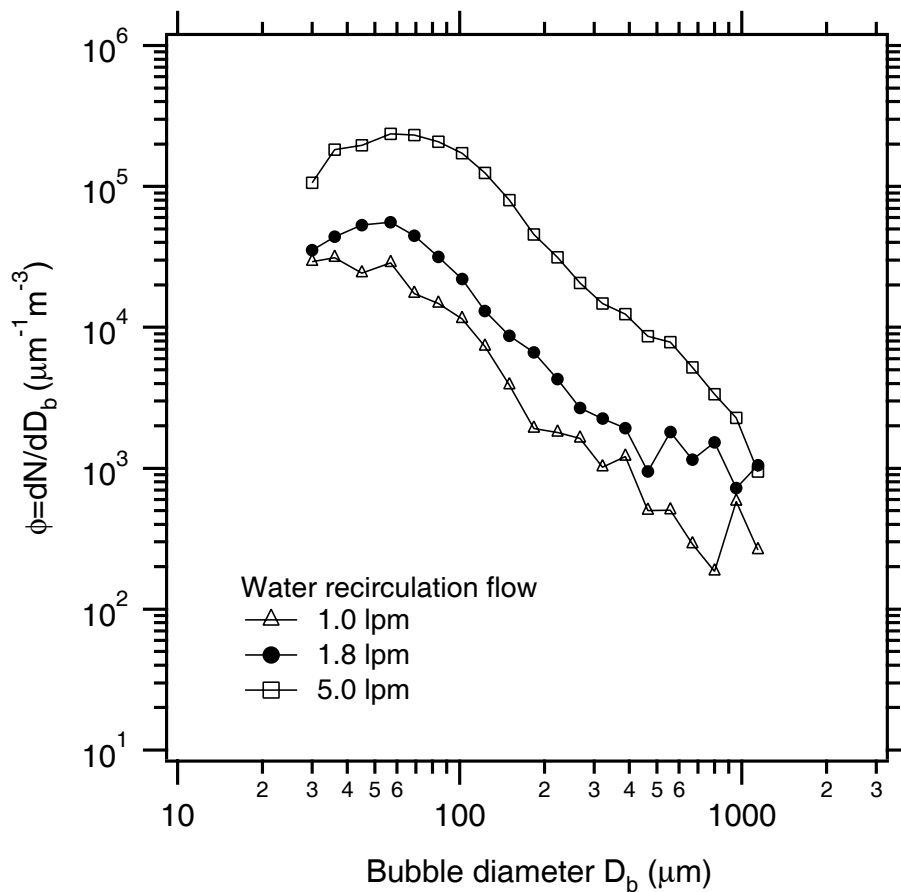


Fig. 3. Bubble population distribution versus bubble diameter for the plume generated by the plunging-water jet system at different water recirculation flows.

[Title Page](#)[Abstract](#)[Introduction](#)[Conclusions](#)[References](#)[Tables](#)[Figures](#)[◀](#)[▶](#)[◀](#)[▶](#)[Back](#)[Close](#)[Full Screen / Esc](#)[Printer-friendly Version](#)[Interactive Discussion](#)

Laboratory-generated primary marine aerosol

E. Fuentes et al.

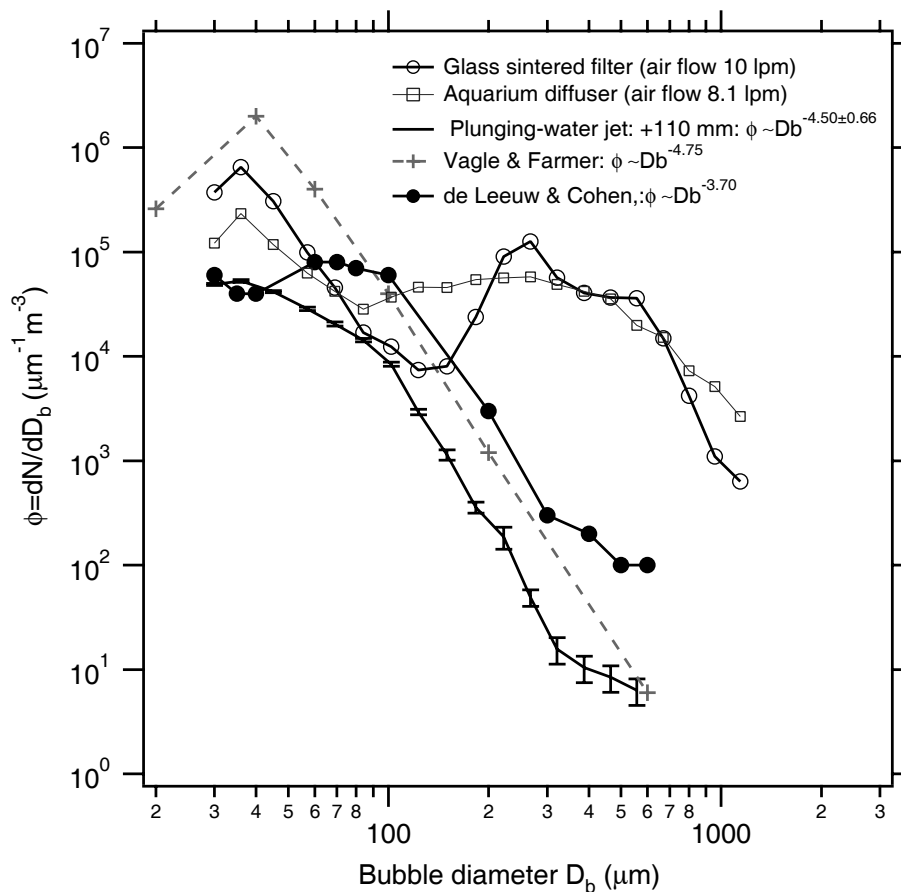


Fig. 4. Comparison of bubble populations obtained in this study with oceanic quiescent bubble spectrum profiles of Vagle and Farmer (1992) and de Leeuw and Cohen (2002).

[Title Page](#)
[Abstract](#)
[Introduction](#)
[Conclusions](#)
[References](#)
[Tables](#)
[Figures](#)
[◀](#)
[▶](#)
[◀](#)
[▶](#)
[Back](#)
[Close](#)
[Full Screen / Esc](#)
[Printer-friendly Version](#)
[Interactive Discussion](#)


Laboratory-generated primary marine aerosol

E. Fuentes et al.

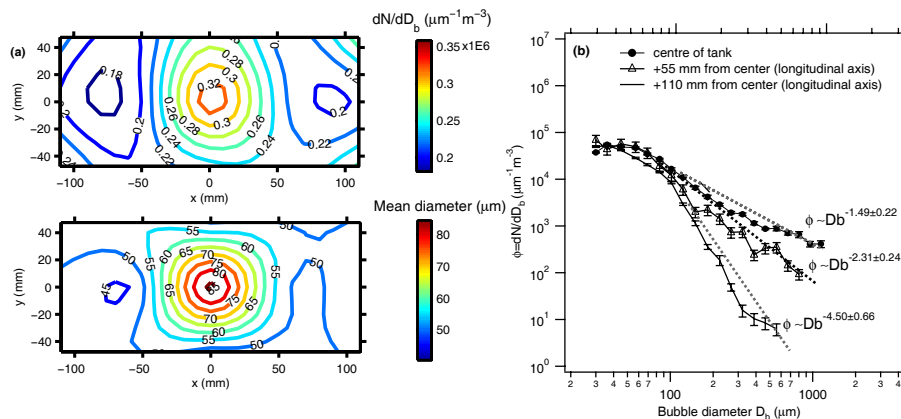


Fig. 5. (a) Spatial distribution of total number and mean size of bubbles generated by the plunging-waterjet system at 1.8 lpm water recirculation flow and (b) bubble spectrums at impingement, +55 mm and +110 mm from the tank centre.

Title Page

Abstract

Introduction

Conclusions

References

Tables

Figures

◀

▶

◀

▶

Back

Close

Full Screen / Esc

Printer-friendly Version

Interactive Discussion



Laboratory-generated primary marine aerosol

E. Fuentes et al.

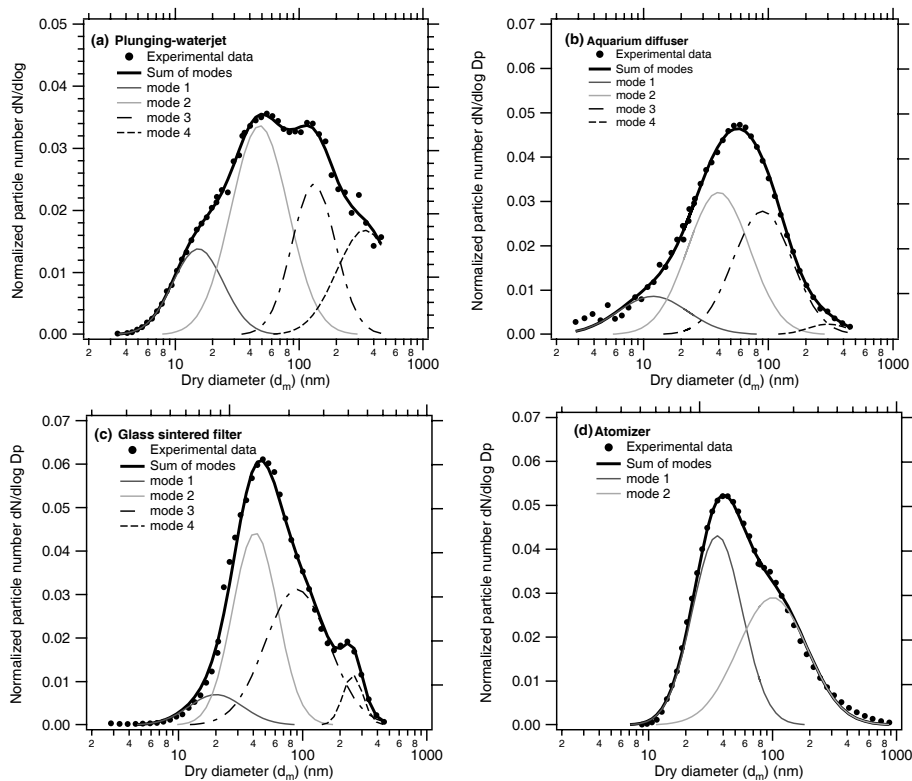


Fig. 6. Normalized particle size distributions of aerosols generated from artificial seawater by (a) the plunging-water jet system (8 water jets), (b) aquarium diffuser (8 lpm air flow), (c) glass sintered filter (5 lpm air flow) and (d) atomizer.

[Title Page](#)[Abstract](#)[Introduction](#)[Conclusions](#)[References](#)[Tables](#)[Figures](#)[◀](#)[▶](#)[◀](#)[▶](#)[Back](#)[Close](#)[Full Screen / Esc](#)[Printer-friendly Version](#)[Interactive Discussion](#)

Laboratory-generated primary marine aerosol

E. Fuentes et al.

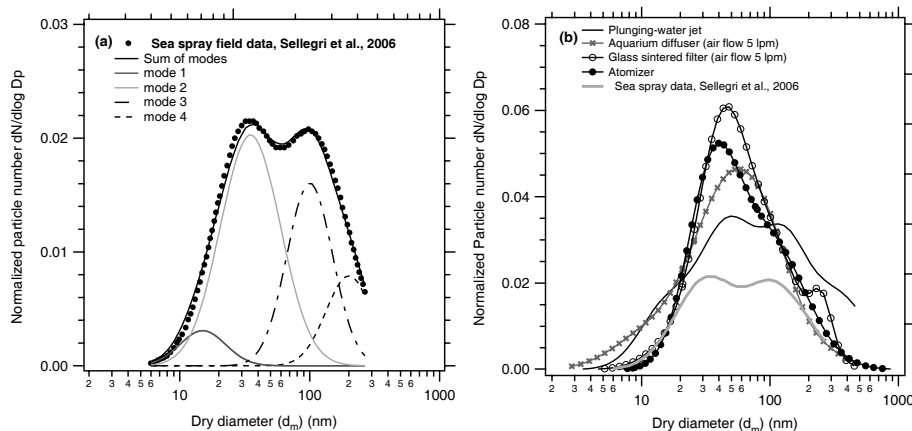


Fig. 7. (a) Normalized atmospheric size distribution from Sellegri et al. (2006) and (b) comparison of normalized particle size distributions of aerosols generated from artificial sea water via bubble-bursting and atomization and the field measurement by Sellegri et al. (2006).

[Title Page](#)[Abstract](#)[Introduction](#)[Conclusions](#)[References](#)[Tables](#)[Figures](#)[◀](#)[▶](#)[◀](#)[▶](#)[Back](#)[Close](#)[Full Screen / Esc](#)[Printer-friendly Version](#)[Interactive Discussion](#)

Laboratory-generated primary marine aerosol

E. Fuentes et al.

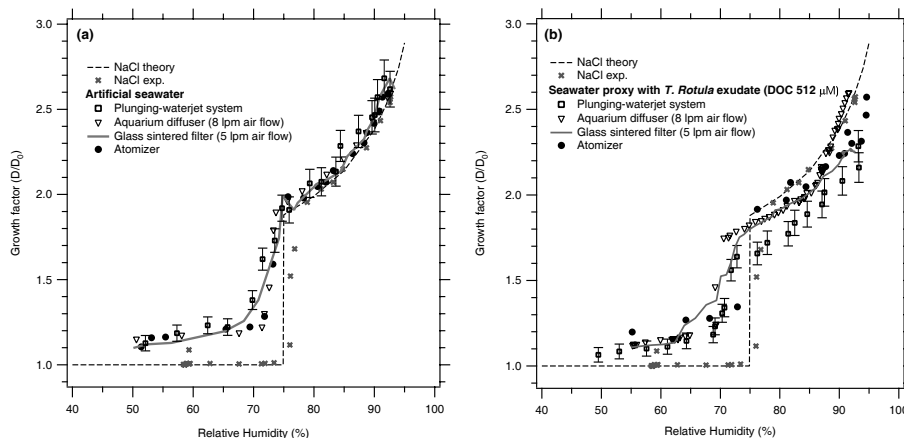


Fig. 8. Humidograms of 100 nm dry particles (d_m) generated from (a) organics-free artificial seawater and (b) natural seawater proxies containing *Thalassiosira Rotula* exudate (DOC 512 μM), via bubble-bursting and atomization. Error bars indicate the uncertainty in the diameter selected by the DMA as function of the shape factor correction in the range from spherical ($\chi=1$) to cubic ($\chi=1.08$) particles.

Title Page

Abstract

Introduction

Conclusions

References

Tables

Figures

◀

▶

◀

▶

Back

Close

Full Screen / Esc

Printer-friendly Version

Interactive Discussion



Laboratory-generated primary marine aerosol

E. Fuentes et al.

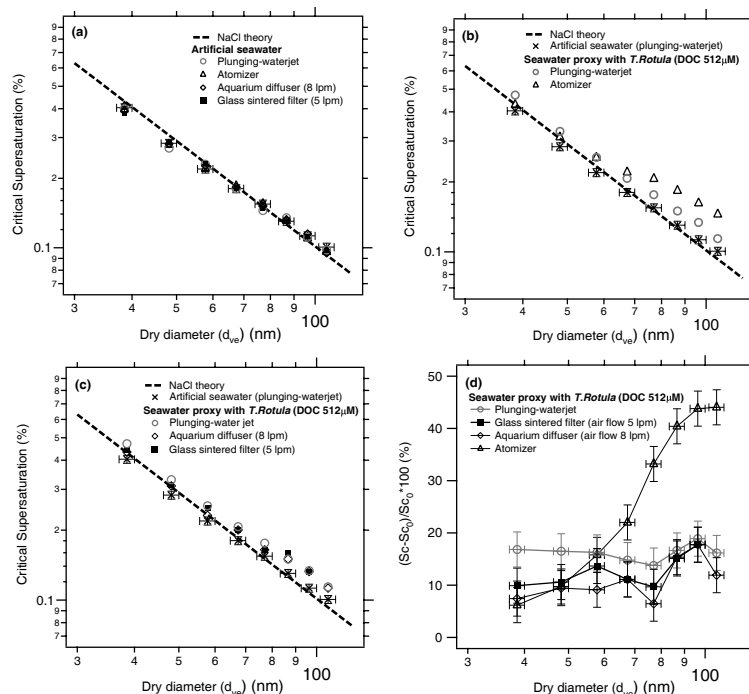


Fig. 9. Critical supersaturation as a function of particle diameter (d_{ve}) for the aerosol generated (a) from artificial seawater and (b), (c) from seawater proxies containing *Thalassiosira Rotula* exudate (DOC 512 μ M) for the different aerosol generation techniques. (d) Relative variation in the critical supersaturation S_c with respect to the critical supersaturation for the case without organics S_{c_0} of aerosols generated from natural seawater containing algal exudate. Horizontal error bars indicate the uncertainty in the diameter selected by the DMA as function of the shape factor correction in the range from spherical ($\chi=1$) to cubic ($\chi=1.08$) shape. Vertical bars indicate the uncertainty in the determination of the critical supersaturation taken as $\pm 1\sigma$ standard deviation.

Title Page

Abstract

Introduction

Conclusions

References

Tables

Figures



Back

Close

Full Screen / Esc

Printer-friendly Version

Interactive Discussion



Laboratory-generated primary marine aerosol

E. Fuentes et al.

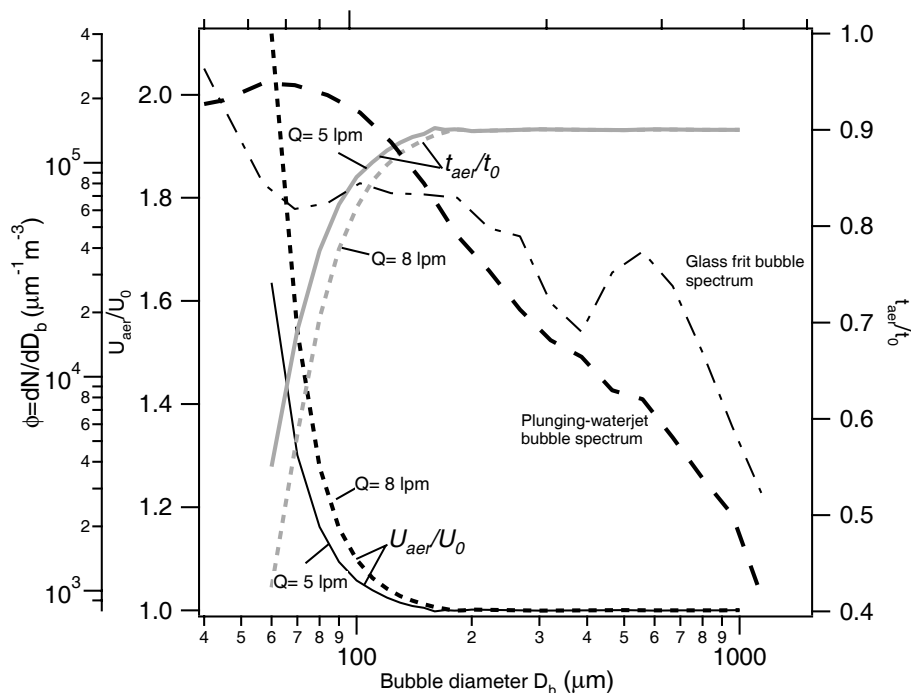


Fig. 10. Glass frit to plunging-water jet bubble rising velocity ratio (U_{aer}/U_0) and residence time ratio (t_{aer}/t_0) for two different aeration flows as a function of bubble size. Bubble population distributions generated by the glass frit (5.2 lpm air flow) and the plunging-water jet (5 lpm water flow) are included for comparison.

Title Page

Abstract

Introduction

Conclusions

References

Tables

Figures

◀

▶

◀

▶

Back

Close

Full Screen / Esc

Printer-friendly Version

Interactive Discussion

